physical evidence was available, similar reaction mechanisms have been proposed for NO_3^- reduction in the presence of GR (*9*, *10*).

We conclude that Se(VI) reduces to Se(IV) and Se(0) in the presence of GR. Although elemental Fe and $Fe(OH)_2$ are absent in nature, their reactions with Se(VI) in the laboratory produced similar redox transformations (*15*, *19*). Thermodynamically, Se(VI) should reduce to the most stable Se(−II) form in the presence of Fe(II), but we did not observe this species at high concentration. However, it can be a dominant species when the Fe(II) concentration is much higher and the reaction times are longer than those we considered. Se(VI) reduction by coprecipitation and adsorption pathways can occur when anoxic conditions are created in Se-contaminated sediments (*16*) [reductive dissolution of Fe(III) oxides precipitates GR with Se], as compared with the ion movement into the previously existing anoxic zones containing GR (dominantly adsorption). The Se(VI) transformation rates we measured are within the range of those reported from other laboratory and field studies on Se speciation in sediments and soils (*20*–*23*). The pore waters of several natural samples are also saturated with respect to GR, which indicates its probable presence in these systems. The rapid precipitation kinetics (*13*) and the flexible crystal structure of GR (*24*) may allow its formation under a variety of geochemical conditions. The reductive dissolution of Fe(III)-oxyhydroxides forms GR steadily in the anoxic sediments; hence, the concentration and final oxidation products of GR are not the limiting factors for the trace element redox reactions. GR-mediated redox reactions similar to those presented here can occur for other trace elements. For instance, studies on Cr(VI) and As(V) reduction have identified the importance of sediment Fe(II)-containing mineral phases as mediators of redox reactions, but attempts to identify these mineral phases are not complete (*25*, *26*). The rapid oxidation of GR poses a problem for its identification during conventional sediment mineralogical analysis, and for this reason this mineral has not been commonly recorded in sediments. However, recent thermodynamic and spectroscopic studies give direct evidence for the existence of GR in soils (*8*, *13*). The abiotic redox reactions we present provide direct evidence for the formation of reduced Se species in anoxic sediments. Although various strains of bacteria have been identified to facilitate Se(VI) reduction in soil and sediment systems, abiotic reactions with GR should be considered when evaluating trace element and major element redox dynamics in sediments and soils.

REFERENCES AND NOTES

1. G. Sposito, *The Chemistry of Soils* (Oxford Univ. Press, New York, 1989).
2. G. A. Cutter, *Science* **217**, 829 (1982).
3. J. H. Howard III, *Geochim. Cosmochim. Acta* **41**, 1665 (1977).
4. H. M. Ohlendorf, D. J. Hoffman, M. K. Saiki, T. W. Aldrich, *Sci. Total Environ.* **52**, 49 (1986).
5. A. M. Shaker, *J. Colloid Interface Sci.* **180**, 225 (1996).
6. R. S. Oremland *et al.*, *Environ. Sci. Technol.* **24**, 1157 (1990).
7. C. Garbisu, T. Ishii, T. Leighton, B. B. Buchanan, *Chem. Geol.* **132**, 199 (1996).
8. F. Trolard *et al.*, *Geochim. Cosmochim. Acta* **61**, 1107 (1997).
9. H. C. B. Hansen, C. B. Koch, H. Nancke-Krogh, O. K. Borggaard, J. Sørenson, *Environ. Sci. Technol.* **30**, 2053 (1996).
10. C. J. Ottley, W. Davison, W. Edmunds, *Geochim. Cosmochim. Acta* **61**, 1819 (1997).
11. K. B. Krauskopf, *Introduction to Geochemistry* (McGraw-Hill, New York, 1979).
12. F. M. M. Morel and J. G. Hering, *Principles and Applications of Aquatic Chemistry* (Wiley Interscience, New York, 1993).
13. H. C. B. Hansen, O. K. Borggaard, J. Sørensen, *Geochim. Cosmochim. Acta* **58**, 2599 (1994).
14. J. M. Bigham and O. H. Tuovinen, in *Planetary Ecology*, D. E Caldwell, Ed. (Van Nostrand Reinhold, New York, 1985), pp. 239–250.
15. S. C. B. Myneni and G. E. Brown Jr., "Stanford Synchrotron Radiation Laboratory Activity Report" (Stanford University, Stanford, CA, 1997).
16. I. J. Pickering, G. E. Brown Jr., T. K. Tokunaga, *Environ. Sci. Technol.* **29**, 2456 (1995).
17. M. E. Essington, *Soil Sci. Soc. Am. J.* **52**, 1574 (1988).
18. D. Rai, A. R. Felmy, D. A. Moore, *J. Solution Chem.* **24**, 735 (1995).
19. R. A. Zingaro, D. C. Dufner, A. P. Murphy, C. D. Moody, *Environ. Int.* **23**, 299 (1997).
20. G. R. Jayaweera and J. W. Biggar, *Soil Sci. Soc. Am. J.* **60**, 1056 (1996).
21. G. Sposito *et al.*, *ibid.* **55**, 1597 (1991).
22. T. K. Tokunaga, I. J. Pickering, G. E. Brown Jr., *ibid.* **60**, 781 (1996).
23. P. H. Masscheleyn, R. D. Delaune, W. H. Patrick Jr., *Environ Sci. Technol.* **24**, 91 (1989).
24. I. R. McGill, B. McEnaney, D. C. Smith, *Nature* **259**, 200 (1976).
25. L. D. Anderson, D. B. Kent, J. A. Davis, *Environ Sci. Technol.* **28**, 178 (1994).
26. J. M. Brannon and W. H. Patrick Jr., *ibid.*, p. 450.
27. The images of mineral grains in 10-μm-thick films of reaction solutions were taken with the high-resolution zone plate microscope, XM-1, which was built and is operated by the Center for X-ray Optics, Lawrence Berkeley National Laboratory (LBNL), Berkeley, CA. See also W. Meyer-Ilse *et al.*, *Synchrotron Radiat. News* **8**, 29 (1995).
28. We thank S. M. Benson, J. M. Bigham, G. Sposito, S. J. Traina, G. A. Waychunas, and P. T. Zawislanski for reviewing the manuscript; M. Zavarin and A. Foster for helping with XAS measurements; and W. Meyer-Ilse and J. T. Brown for their collaboration with x-ray microscopy studies. Supported by the Office of Basic Energy Science, Geoscience Program, grant DOE: DE-ACO3-76SF00098 (to T.K.T. and S.C.B.M.); Laboratory Directed Research and Development Fund, LBNL (to S.C.B.M.); and NSF grant EAR-9406490 (to G.E.B.). The Stanford Synchrotron Radiation Laboratory and the Center for X-ray Optics and Advanced Light Source (LBNL) are funded by the U.S. Department of Energy. This is LBNL journal article number LBNL-40832/UC-03.

22 July 1997; accepted 24 September 1997

High-Pressure Transformation of Al_2O_3

Nobumasa Funamori and Raymond Jeanloz

X-ray diffraction measurements indicate that ruby (Cr^{3+} doped α-Al_2O_3) transforms to the Rh_2O_3 (II) structure when heated to temperatures exceeding ~1000 kelvin at pressures above ~100 gigapascals, in agreement with predictions from ab initio quantum mechanical calculations. The high-pressure phase did not quench upon decompression to ambient pressure, and the occurrence of this phase transformation may affect interpretations of static (diamond-anvil cell) and dynamic (shock-wave) experiments at ultrahigh pressures.

Corundum (α-Al_2O_3, space group $R\bar{3}c$) is important in many fields of research, for example serving as a model material in ceramic science (*1*). In high-pressure research, it is used as a window in shock-wave experiments (*2*), and also as a pressure-transmitting medium for static compression in the diamond-anvil cell (DAC) (*3*). Moreover, the pressure-induced shift of the Cr^{3+} fluorescence wavelength of ruby (Cr^{3+} doped α-Al_2O_3) is used as a pressure calibrant in DAC experiments (*4*). Theoretical calculations on the behavior of corundum at high pressures (*5*–*7*) predict that α-Al_2O_3 will transform to the Rh_2O_3 (II) structure (space group *Pbcn*) (*8*). Recent calculations, based either on pseudopotential (*7*) or on linearized augmented plane-wave (*6*) methods, yield a transition pressure of 78 to 91 GPa, raising the possibility that the ruby-fluorescence pressure scale may be contaminated by the effects of a structural transformation. However, no evidence of a transformation was observed in a high-pressure x-ray diffraction study on ruby to 175 GPa (*9*), and it has therefore been assumed that the α-Al_2O_3 structure is stable to this pressure.

To clarify whether there is a transformation, we carried out a high-pressure in situ x-ray diffraction experiment on ruby that had been heated to a temperature exceeding ~1000 K while at high pressure (*10*).

Department of Geology and Geophysics, University of California, Berkeley, CA 94720-4767, USA.

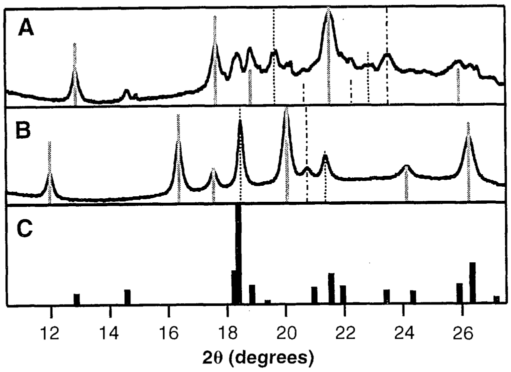

Fig. 1. X-ray diffraction patterns of a mixture of Al_2O_3 and Pt (and Fe gasket) (**A**) obtained under pressure after heating (see Table 2 for pressure conditions), (**B**) obtained subsequently after decompression to ambient pressure, and (**C**) calculated for the Rh_2O_3 (II) phase (Table 1). Gray, dotted, and dashed lines indicate the calculated diffraction patterns for α-Al_2O_3, Pt, and Fe [ε-phase in (A) and α-phase in (B)], respectively.

Heating the sample is often necessary to overcome kinetic barriers to transformation (*11*). The sample was not heated in the previous study of ruby up to 175 GPa (*9*). Here, the sample consisted of polycrystalline ruby mixed with Pt (5 wt%), which acts as an absorber of the laser beam for heating and as a pressure standard (*12*). Using the ruby-fluorescence technique (*4*), we measured a pressure of ~100 GPa before heating; probably because of nonhydrostaticity, the R_1 fluorescence line of ruby was broad and weak (*4*, *9*), so that the uncertainty in pressure is large (± 10 GPa). After heating, the fluorescence line became weaker, and pressure could no longer be reliably determined using the ruby. This is in contrast to the effect of heating ruby below 70 to 80 GPa: In these cases, laser heating typically causes a pressure relaxation of 10 (± 5) GPa, reducing the degree of nonhydrostaticity such that pressure can be measured more easily than before heating (*13*).

The high-pressure x-ray diffraction pattern obtained after heating the sample exhibits lines that can be assigned to a different phase of Al_2O_3, along with lines for α-Al_2O_3 [untransformed sample material (*14*)], Pt, and ε-Fe (gasket) (Fig. 1A). In contrast, all diffraction lines observed after decompression can be assigned to α-Al_2O_3, Pt, and α-Fe (gasket), with no evidence of the high-pressure phase being present (Fig. 1B). The disappearance of diffraction lines on decompression proves that we created a high-pressure phase that is not stable at low pressures. By comparing the lines that were only observed under high pressure with the diffraction pattern predicted for the Rh_2O_3 (II) structure, we determined orthorhombic unit-cell parameters (Table 1). Using these parameters and the theoretically obtained internal positions for Al and O (*15*), we calculated the diffraction pattern for Rh_2O_3 (II) (Fig. 1C). Except for a few lines, the high-pressure pattern is explained as a combination of α- and Rh_2O_3 (II) forms of Al_2O_3, along with Pt and ε-Fe. The origin of the unexplained lines is not clear, but their presence might indicate the existence of an additional phase. It is also possible that the high-pressure phase that we have tentatively assigned to Rh_2O_3 (II) has a different structure. However, because the diffraction pattern of the recovered sample consists of only α-Al_2O_3 and Pt lines (and one α-Fe line from the gasket), it is unlikely that chemical reactions occurred in our experiment.

Pressures calculated for the α-Al_2O_3 and Pt phases give about the same value (Table 2) and are compatible with the pressure estimated from the ruby-fluorescence method, if the relaxation of pressures by heating is taken into account. The pressure obtained using ε-Fe is lower than the pressure calculated for α-Al_2O_3 and Pt (Table 2), but the effect of uniaxial stress [up to 10 to 15 GPa estimated from (*16*)] and radial pressure gradients (*9*, *13*) can explain this difference. The volume decrease due to transformation from α-Al_2O_3 to Rh_2O_3 (II) structures was predicted to be 2.2% (*7*), whereas our experimental value is 3.8%. This difference can be explained by a ~10 GPa pressure difference between the two phases; the Rh_2O_3 (II) structure may have been subjected to a higher pressure than α-Al_2O_3 (for example, if only the highest pressure region of the sample transformed). Moreover, the *a*/*c* and *b*/*c* ratios of lattice parameters obtained for the Rh_2O_3 (II) structure, 1.414 and 0.969, are close to the theoretical values of 1.419 and 0.973, respectively (*7*).

The agreement between observed and theoretically predicted unit-cell parameters leads us to conclude that α-Al_2O_3 transforms to a high-pressure phase, probably with the Rh_2O_3 (II) structure, by ~100 GPa (*17*). This finding supports the predictions of ab initio calculations (*5*-*7*) and substantiates potential concerns about using the ruby-fluorescence method of calibrating pressures in samples heated at ultra-high pressures (*18*). Also, lines from the Rh_2O_3 (II) phase of a ruby calibrant or a pure Al_2O_3 pressure-transmitting medium could be misinterpreted as indicating a phase transformation of the sample itself in ultra-high-pressure x-ray diffraction experiments.

Finally, defect production associated with the phase transition could explain the rise in opacity and decrease in electrical resistivity that has been reported in pure Al_2O_3 under shock-compression (*2*, *19*). These defects can give a nonthermal contribution to the spectrum emitted by Al_2O_3, which is used as a window material for spectroradiometric shock-temperature measurements at ultra-high pressures. Furthermore, our results confirm that anomalously low shock-wave velocities obtained in Hugoniot measurements on Al_2O_3 between 80 and 340 GPa can be attributed to the polymorphic phase transformation (*20*).

Table 1. Observed and calculated* *d*-values for the high-pressure phase of Al_2O_3.

h k l	d_{obs} (Å)	d_{calc} (Å)	$d_{obs}/d_{calc} - 1$
111	2.8632	2.8655	−0.0008
002	2.2917	2.2950	−0.0014
211	2.2744	2.2759	−0.0007
021	2.0019	2.0011	0.0004
121	1.9105	1.9122	−0.0009
212	1.7278	1.7266	0.0007
022	1.5977	1.5969	0.0005
122	1.5508	1.5506	0.0001

*a = 6.488(12) Å, b = 4.447(3) Å, c = 4.590(4) Å, V = 132.4(3) $Å^3$, with uncertainties in the last decimal places indicated in parentheses.

Table 2. Unit-cell parameters and pressures are determined from high-pressure x-ray diffraction pattern. Uncertainties in the last decimal places are indicated in parentheses. Equations of state used in pressure calculations are from (*9*), (*12*), and (*22*) for α-Al_2O_3, Pt, and ε-Fe, respectively.

Phase	*a* (Å)	*c* (Å)	Pressure (GPa)
α-Al_2O_3	4.4485(7)	12.046(3)	86.1
Pt	3.677(10)	–	89.4
ε-Fe	2.3422(2)	3.7698(4)	65.9

REFERENCES AND NOTES

1. R. H. Insley, in *Alumina Chemicals Science and Technology Handbook*, L. D. Hart, Ed. (American Chemical Society, Westerville, OH, 1990), pp. 293–297.
2. S. T. Weir, A. C. Mitchell, W. J. Nellis, *J. Appl. Phys.* **80**, 1522 (1996).
3. R. Boehler, *Nature* **363**, 534 (1993).
4. H. K. Mao, P. M. Bell, J. W. Shaner, D. J. Steinberg, *J. Appl. Phys.* **49**, 3276 (1978).
5. R. E. Cohen, *Geophys. Res. Lett.* **14**, 37 (1987); H. Cynn, D. G. Isaak, R. E. Cohen, M. F. Nicol, O. L. Anderson, *Am. Mineral.* **75**, 439 (1990); M. S. T. Bukowinski, A. Chizmeshya, G. H. Wolf, H. Zhang, *Mol. Eng.* **6**, 81 (1996).
6. F. C. Marton and R. E. Cohen, *Am. Mineral.* **79**, 789 (1994).
7. K. T. Thomson, R. M. Wentzcovitch, M. S. T. Bukowinski, *Science* **274**, 1880 (1996).
8. R. D. Shannon and C. T. Prewitt, *J. Solid State Chem.* **2**, 134 (1970).
9. A. P. Jephcoat, R. J. Hemley, H. K. Mao, *Physica B* **150**, 115 (1988).

10. A gasketed Mao-Bell type DAC was used with anvils having 200-μm culets [H. K. Mao, P. M. Bell, K. J. Dunn, R. M. Chrenko, R. C. DeVries, *Rev. Sci. Instrum.* **50**, 1002 (1979)]. The gasket was spring steel, and the sample diameter under pressure was ~80 μm. The sample was heated by means of a continuous (cw) Nd:YAG (Nd:yttrium-aluminum-garnet) laser operating in multi-mode (wavelength of 1064 nm), as described by A. Kavner and R. Jeanloz [in *Advanced Materials '96*, M. Akaishi *et al.*, Eds. (NIRIM, Tsukuba, Japan, 1996), pp. 143–147]. The laser beam was focused to a diameter of ~15 μm and scanned to heat the entire sample. X-ray diffraction patterns were collected in angular-dispersive mode at beamline 10-2 of the Stanford Synchrotron Radiation Laboratory (SSRL), using a monochromatized x-ray beam of 17.038 keV with an imaging-plate detector. Because the diameter of the incident x-ray beam was slightly larger than that of the sample, diffraction line or lines from the gasket were present in the patterns we collected. The imaging-plate data were converted to a 2θ-intensity profile, using the program developed by J. H. Nguyen and R. Jeanloz [*Rev. Sci. Instrum.* **64**, 3456 (1993)]. All x-ray diffraction measurements were carried out at room temperature.
11. See, for example, W. A. Caldwell *et al.*, *Science* **277**, 930 (1997).
12. Because the equation of state of Pt is well known, pressure can be calculated from the unit-cell volume of Pt measured by x-ray diffraction [N. C. Holmes, J. A. Moriarty, G. R. Gathers, W. J. Nellis, *J. Appl. Phys.* **66**, 2962 (1989)].
13. See, for example, D. Heinz and R. Jeanloz, *J. Geophys. Res.* **92**, 11437 (1987).
14. Pressure or temperature gradients, or both, in the sample chamber (*9*, *13*) may have resulted in the existence of untransformed α-Al_2O_3.
15. $Al^{(1)}$ = (0.110, 0.753, 0.032), $O^{(1)}$ = (0.846, 0.607, 0.102), $O^{(2)}$ = (0.000, 0.049, 0.250) (*7*).
16. R. J. Hemley *et al.*, *Science* **276**, 1242 (1997). Because we did not heat the gasket, it may have retained a large uniaxial stress.
17. Transformations from α-Al_2O_3 to phases of unknown structure at 16 to 21 GPa and 1600 to 1900 K have been proposed, based on optical observations on quenched samples [T. Gasparik, *J. Geophys. Res.* **95**, 15751 (1990)]. Experimental details have not been reported, but the high-pressure phase documented here is likely to be different, because it cannot be quenched to ambient pressure. In a separate experiment, we have tentative evidence for the appearance of the Rh_2O_3 (II) phase when ruby is heated at a pressure as low as ~85 GPa.
18. To avoid such problems in ultra-high pressure experiments with the laser-heated DAC, attempts are usually made to obtain ruby-fluorescence determinations of pressure from portions of the sample that have been heated as little as possible. See E. Knittle and R. Jeanloz, *Science* **235**, 668 (1987); Q. Williams, E. Knittle, R. Jeanloz, *J. Geophys. Res.* **96**, 2171 (1991); (*3*); and (*7*).
19. P. A. Urtiew, *J. Appl. Phys.* **45**, 3490 (1974); C. S. Yoo, N. C. Holmes, M. Ross, D. J. Webb, C. Pike, *Phys. Rev. Lett.* **70**, 3931 (1993).
20. D. Erskine's [in *High-Pressure Science and Technology—1993*, part I, S. C. Schmidt *et al.*, Eds. (American Institute of Physics, Woodbury, NY, 1994), pp. 141–143] shock-wave equation of state (Hugoniot) measurements on single-crystal Al_2O_3 are described by $U_S = 8.74 + 0.96\ u_p$ between 80 and 340 GPa, where U_S and u_p are shock-wave velocity and particle velocity, respectively, and all values are in km/s. On the basis of its elastic properties (*9*, *21*), α-Al_2O_3 is expected to follow $U_S = 7.93 + 1.32\ u_p$ [see R. Jeanloz, *J. Geophys. Res.* **94**, 5873 (1989)], and the data of (*21*) are found to be compatible with this for u_p between about 1.6 and 2.5 km/s (strength effects probably explain higher shock-wave velocities for $u_p < 1.6$ km/s). The intersection of these two U_S-u_p relations, $u_p = 2.25$ km/s, can be combined with the Hugoniot momentum-conservation relation to obtain a pressure of 98 GPa at which the shock-wave data begin to deviate toward a new (high-pressure phase) branch of the Hugoniot. This is in good agreement with the pressure at which we find evidence for the crystal-structural transformation of Al_2O_3. Also, a theoretical Hugoniot calculated for the Rh_2O_3 (II) phase matches the U_S-u_p relation measured by Erskine for Al_2O_3 at pressures above 100 GPa.
21. S. P. Marsh, Ed., *LASL Shock Hugoniot Data* (Univ. of California Press, Berkeley, CA, 1980).
22. A. P. Jephcoat, H. K. Mao, P. M. Bell, *J. Geophys. Res.* **91**, 4677 (1986).

23. We are grateful to M. S. T. Bukowinski, T. Uchida, J. H. Nguyen, W. A. Caldwell, L. R. Benedetti, and staff members at SSRL for helpful discussions and experimental support. Supported by NSF, NASA, and the Miller Institute for Basic Research in Science (Berkeley, CA).

5 August 1997; accepted 7 October 1997

Direct Measurement of Distances and Angles in Biomolecules by NMR in a Dilute Liquid Crystalline Medium

Nico Tjandra and Ad Bax

In isotropic solution, internuclear dipolar couplings average to zero as a result of rotational diffusion. By dissolving macromolecules in a dilute aqueous nematic discotic liquid-crystalline medium containing widely spaced magnetically oriented particles, a tunable degree of solute alignment with the magnetic field can be created while retaining the high resolution and sensitivity of the regular isotropic nuclear magnetic resonance (NMR) spectrum. Dipolar couplings between ^1H-^1H, ^1H-^{13}C, ^1H-^{15}N, and ^{13}C-^{13}C pairs in such an oriented macromolecule no longer average to zero, and are readily measured. Distances and angles derived from dipolar couplings in human ubiquitin are in excellent agreement with its crystal structure. The approach promises to improve the accuracy of structures determined by NMR, and extend the size limit.

Internuclear magnetic dipole couplings contain a great deal of structural information, but in isotropic solution, they average to zero as a result of rotational diffusion. However, their effect on nuclear spin relaxation results in measurable nuclear Overhauser effects (NOEs). These NOEs are commonly interpreted in terms of qualitative internuclear distances, which constitute the basis for macromolecular structure determination by NMR (*1*). The qualitative manner in which interprotein distances are derived from NOEs limits the accuracy at which the time-averaged conformation of biomolecules can be determined. Moreover, the cumulative error in these local constraints can make it difficult to determine the relative positions of structural elements with few connecting NOEs.

These problems can be addressed by making use of the minute degree of molecular alignment that occurs for proteins with a nonzero magnetic susceptibility anisotropy when they are placed in a strong magnetic field (*2*–*5*). Such alignment can result in measurable values of the one-bond ^{15}N-^1H and ^{13}C-^1H dipolar couplings. Because the internuclear distance for these dipolar interactions is essentially fixed, the dipolar couplings provide direct information on the orientations of the corresponding bond vectors relative to the protein's magnetic susceptibility tensor. These constraints are therefore fundamentally different from the strictly local NOE and *J* coupling constraints. Addition of only 90 such dipolar constraints, measured for a small protein complexed with a 16–base pair DNA fragment, resulted in a nearly twofold reduction of ϕ-ψ pairs (torsion angles) outside of the most-favored region of the Ramachandran map (*5*) and greatly improved the agreement between predicted and measured magnetic field dependence of ^{15}N shifts (*6*). Unfortunately, the magnetic interaction energy for an individual macromolecule is generally so weak that only in favorable systems, and with considerable effort, can these dipolar couplings be measured with sufficient accuracy. Here we demonstrate a simple and general method for inducing alignment of biomolecules with the magnetic field: the use of an aqueous, dilute, liquid crystalline (LC) phase. This method yields an adjustable degree of molecular alignment and allows not only ^1H-^{15}N, but also many other types of dipolar interactions to be measured directly and with high accuracy.

Although LC media have long been used for orienting solutes in order to study their structure (*7*–*9*), the degree of solute orientation typically obtained in such a sol-

---

N. Tjandra, Laboratory of Biophysical Chemistry, National Heart, Lung, and Blood Institute, National Institutes of Health, Bethesda, MD 20892–0380, USA.
A. Bax, Laboratory of Chemical Physics, National Institute of Diabetes and Digestive and Kidney Diseases, National Institutes of Health, Bethesda, MD 20892–0520, USA.